PERGAMON

Building and Environment 34 (1999) 377–389

BUILDING AND ENVIRONMENT

Modelling of emission of volatile organic compounds from building materials—estimation of gas-phase mass transfer coefficient

Fariborz Haghighat*, Ying Zhang

School for Building, Concordia University, Montreal, Quebec, Canada

Received 2 September 1997; revised 26 February 1998; accepted 2 June 1998

Abstract

A mathematical model is developed to predict Volatile Organic Compound (VOC) emission rates from homogeneous materials. The model considers both mass diffusion and mass convection processes in the boundary layer between the material surface and the air flow. Establishing the relationship between the surface air flow and emission rate; the model, therefore can predict the material emission rate under different environmental conditions. The other feature of the model is that all the parameters have clear physical meaning and can be either found in literature or calculated using known theories and/or equations.

The prediction of the mathematical model was validated at three different levels; with experimental results from the CBS specially designed test chamber, with experimental results from the EPA which were carried out in an ASTM chamber, and finally with the predictions made by other models. The results indicate that there is, in general, good agreement between the model predictions and the experimental results. The main advantage of this model is that the model does not require any experimental data as input.

Keywords: Model; Emission rate; Indoor air quality; Velocity; VOC

1. Introduction

There has been growing interest in the development of mathematical models to describe the material emission process and the effects of indoor environmental conditions on this process. Several models have been developed and these models can be categorized into two groups: empirical and semi-physical models.

The empirical model is based on fitting an appropriate mathematical expression to a set of experimental data, usually concentration as a function of time [1–3]. The disadvantage of the empirical model is that the coefficients in the equations have to be obtained from experiments for each material and under different environmental conditions, therefore, these coefficients do not have any physical meaning.

The earliest semi-physical models to predict emission rates from materials were proposed by Hoetjer [4] and Black and Bayer [5]. In the development of these models, it was assumed that the internal resistance of materials to mass diffusion was negligible. This assumption restricts the application of the model, where the transport of vapour through a board–air interphase region is a rate limiting process. Dunn proposed a model for the prediction of emissions from a thin film [6]. The main assumption here was that the emission is merely a surface phenomenon. The model considers sink effects, however, the assumption of thin film restricts its application to thick materials where diffusion is a controlling factor.

The latest physical model based on Fick's Law of Diffusion was developed for wet materials by Guo and Tichenor [7]. The following assumptions were made in the development of this model.

(1) For a given wet material, all freshly applied surfaces are assumed to have the same VOC vapour pressure. In other words, vapour pressure is a property of that wet material and is independent of the amount of coating applied. The amount of coating only effects the decay rate; the more material applied, the slower the decay.
(2) The surface VOC concentration during the aging period is proportional to the mass of VOC remaining.
(3) The average diffusivity of the solvent molecules can be represented by the diffusivity of the most abundant component in the solvent mixture.

The preliminary validation of the model indicates that

* Corresponding author. Tel.: 001-514-848-3192; Fax: 001-514-848-7965; E-mail: haghi@cbs-engr.concordia.ca

S0360-1323/99 $ - see front matter
PII: S0360-1323(98)00036-5

the model provides a better fit to experimental results from test chambers than the empirical or other semi-physical models. The main drawback of this model is that the boundary layer thickness has to be obtained through data-fitting the experimental results. Haghighat and De Bellis [8] discussed the impact of temperature and humidity on the emission rate profile of materials. Recently, Sparks et al. [9] proposed a method to estimate the gas-phase mass transfer coefficient based on the fluid dynamic conditions of the environment.

This paper describes a new approach to estimate the gas-phase mass transfer coefficient based on the principles of mass transfer and fluid flow. Also, the paper reports the results of the validation of this model with: experimental results from the velocity-controlled test chamber, experimental results from the EPA which were carried out in an ASTM chamber, and finally with the predictions made by other models.

2. Theoretical background

The material emission rates are determined, partly, by the rates of diffusion from the interior of the material to the surface and, partly, by the VOC transfer rates through the air current in contact with the material surface, as shown in Fig. 1A.

The emission rate can be calculated either based on interior mass transfer or exterior mass transfer, as shown in the following equation:

$$m = h_s(C_o - C_s) = h_m(C_s - C_\infty) \quad (1)$$

where m is the mass emission rate at time t ($mgm^{-2}h^{-1}$), C_s is the surface VOC concentration at time t (mgm^{-3}), C_o is the interior VOC concentration at time t (mgm^{-3}), C_∞ is the VOC concentration in the air flow (mgm^{-3}), h_s is the interior VOC mass transfer coefficient (mh^{-1}), and h_m is the exterior VOC mass transfer coefficient (mh^{-1}).

Interior mass transfer is determined from the physical and chemical properties of materials. The mechanism is so complicated that little is known about it. The exterior material emission process involves evaporation, diffusion, convection, absorption and desorption, etc. According to eqn (1), in order to calculate the VOC emission rates, the surface VOC concentration, C_s, and the exterior mass transfer coefficient, h_m, must first be determined.

2.1. Surface VOC concentration (C_s)

The following basic assumptions are made for calculating the surface VOC concentration:

(1) For any given material, there exists a VOC source characteristic concentration, C_o, which is dependent on the material content, age and structure, but independent of the loading and environmental conditions. The air immediately adjacent to tl material surface has the surface VOC concentratio C_s.
(2) For solid materials, C_s decays very slowly and can b treated as a constant during a certain time period. is proportional to the VOC source concentration, C and a function of temperature and relative humidit and it can be measured by using the static headspa method.

For liquid materials, C_s is the concentration of tl specific VOC and is a function of time $C_s = f(t)$. When wet material is newly applied to a surface, it has an initi VOC concentration of C_{so} near the surface, which is the saturated vapour pressure of the specific VOC. C_{so} a function of temperature and humidity and C_o. As tl wet material ages, the vapour pressure of the remainir VOC decreases gradually [1]. If the fresh surface has VO concentration of C_{so} and an initial mass per unit ar of VOC applied of M_o, (mgm^{-3}), the concentration C (mgm^{-3}), during the aging period is proportional to tl mass of VOC remaining, $M(t)$, (mgm^{-3}).

$$C_s(t) = C_{so}\left(\frac{M(t)}{M_o}\right) \quad (2$$

2.2. Exterior mass transfer coefficient (h_m)

In the case of a room or an enclosure, the air flow clo to the walls is a complex three-dimensional and no isotropic turbulent flow. There is a boundary layer adja ent to each surface by which the VOC exterior ma transfer rate is determined. The mass transfer rates VOCs in the boundary layer are governed by diffusio forced convection, natural convection, and adsorptio /desorption. Numerous parameters have an impact o the emission process. The following assumptions a made:

(1) No chemical reactions, no desorption or adsorptio
(2) Material surfaces have uniform roughness and a thi layer is applied in the case of wet materials.
(3) Steady state stream flow over the surface.
(4) Uniform VOC concentration in ambient air.
(5) No temperature difference between the air an material surfaces.
(6) In the case of TVOC (total volatile organic con pounds) calculation, the diffusivity of the most abu dant component is used as the diffusivity of TVO D.
(7) The static viscosity of the wet material is much larg than the static viscosity of the stream flow $\mu_l \gg \mu_g$.

As there is no temperature difference between the su faces and the air flow over it, the natural convectio caused by buoyancy effects can be neglected. Althoug the densities of different VOCs are higher than that

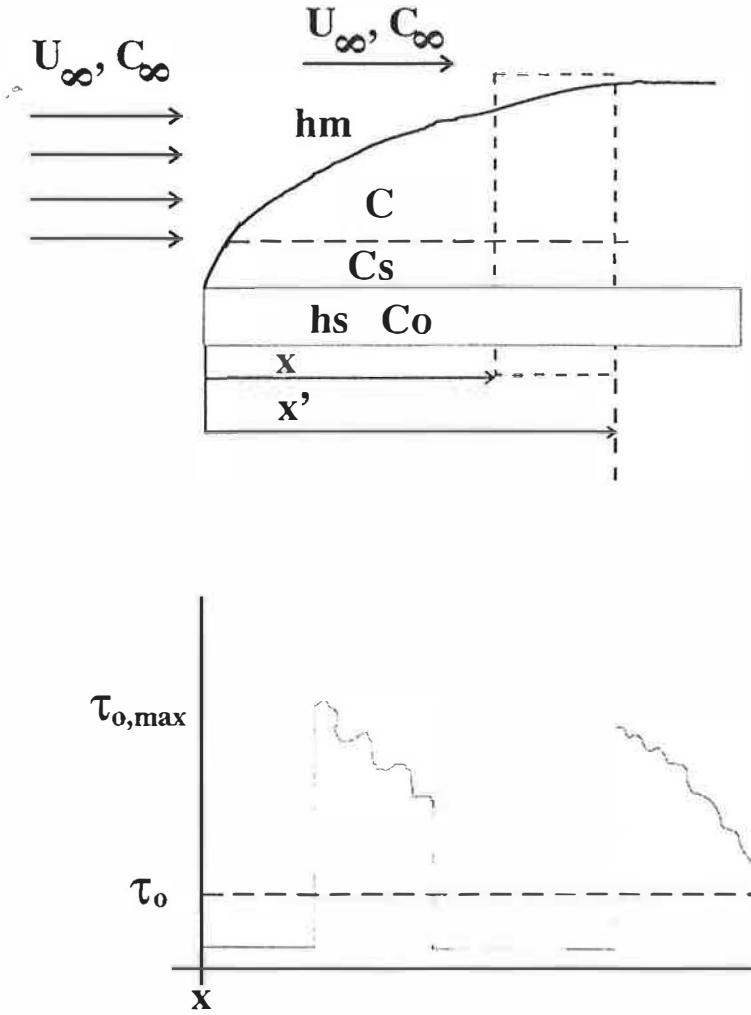

Fig. 1. Schematic of emission process.

air, the migration caused by the gravity force is negligible compared to the migration caused by turbulence and concentration differences. This is due to the relatively small diameters of the VOC molecules and the random collision of VOC and gas molecules [10]. Therefore, there is little difference in flow conditions and mass transfer processes according to the surface orientation. The time-averaged governing equations of fluid flow and mass transfer in the boundary layer for all surfaces in a room or an enclosure can be written as:

Continuity equation:

$$\frac{\partial}{\partial x_i}(\rho u_i) = 0 \tag{3}$$

$$u_i = \bar{u}_i + u_i' \tag{4}$$

where $\bar{u}_i$ is the mean velocity and u_i' is its fluctuating component; j denotes the x, y or z coordinates.

Momentum conservation equation:

$$\frac{\partial u_i u_j}{\partial x_i} = -\frac{1}{\rho}\frac{\partial p}{\partial x_i} + \frac{\partial}{\partial x_i}\left[\frac{\mu}{\rho}\left(\frac{\partial u_i}{\partial x_j} + \frac{\partial u_j}{\partial x_i}\right)\right] \tag{5}$$

where μ is the dynamic viscosity of air, and i and j denote the x, y or z coordinates.

Mass conservation equation:

$$\frac{\partial u_i c}{\partial x_i} = \frac{\partial}{\partial x_i}\left(\rho D \frac{\partial c}{\partial x_i}\right) + S_c \tag{6}$$

$$c = \bar{c} + c' \tag{7}$$

where $\bar{c}$ is the mean concentration, and c' is its fluctuation component, D is the diffusion coefficient of a specific VOC in air, and S_c is the source term.

Although the actual turbulent flow is three-dimensional, regardless of how simple the flow boundaries are, from symmetry, the terms representing the $\partial/\partial x_j$ derivative of time-averaged quantities in eqns (5) and (6) are zero. Furthermore, if u' and v' are treated as the velocity

fluctuations caused by an eddy as it rides along with the mean flow, then u' and v' are of comparable orders of magnitude. This means that in the boundary layer the term $(\partial/\partial x)(u'^2)$ can be neglected relative to $(\partial/\partial y)(u'v')$ in eqn (5), and $(\partial/\partial x)(u'c')$ relative to $(\partial/\partial y)(v'c')$ in eqn (6). Due to the slenderness of the boundary layer, $\delta \ll L$, the momentum and mass conservation equations in the near wall region can be simplified into two dimensional boundary layer equations [11], as follows:

$$\bar{u}\frac{\partial \bar{u}}{\partial x}+\bar{v}\frac{\partial \bar{u}}{\partial y}=-\frac{1}{\rho}\frac{\partial \bar{P}}{\partial x}+\frac{\mu}{\rho}\left(\frac{\partial^2 \bar{u}}{\partial y^2}\right)-\frac{\partial \overline{u'v'}}{\partial y} \tag{8}$$

$$\bar{u}\frac{\partial \bar{c}}{\partial x}+\bar{v}\frac{\partial \bar{c}}{\partial y}=D\left(\frac{\partial^2 \bar{c}}{\partial y^2}\right)-\frac{\partial \overline{v'c'}}{\partial y}. \tag{9}$$

By defining the eddy shear stress and eddy mass flux as:

$$-\rho\overline{u'v'}=\rho\varepsilon\frac{\partial \bar{u}}{\partial y} \tag{10}$$

$$-\rho\overline{v'c'}=\rho\varepsilon_m\frac{\partial \bar{c}}{\partial y} \tag{11}$$

where ε is the eddy kinematic viscosity, and ε_m is the eddy mass diffusivity;
the boundary equations become:

$$\bar{u}\frac{\partial \bar{u}}{\partial x}+\bar{v}\frac{\partial \bar{u}}{\partial y}=-\frac{1}{\rho}\frac{\partial \bar{P}}{\partial y}+\frac{\partial}{\partial y}\left[(\nu+\varepsilon)\frac{\partial \bar{u}}{\partial y}\right] \tag{12}$$

$$\bar{u}\frac{\partial \bar{c}}{\partial x}+\bar{v}\frac{\partial \bar{c}}{\partial y}=\frac{\partial}{\partial y}\left[(D+\varepsilon_m)\frac{\partial \bar{c}}{\partial y}\right] \tag{13}$$

where the boundary conditions for velocity and concentration are U_∞ and C_∞ at the free stream respectively, and zero ($U=v=0$) and C_s at the material surface, respectively.

Based on the theory of fluid dynamics, both velocity and concentration boundary layers on a non-slip solid surface have been visualized as two sublayers: (1) the viscous sublayer, where $\nu \gg \varepsilon$, and (2) the fully turbulent sublayer, where $\varepsilon \gg \nu$. The two sublayers merge at some place where ν and ε are of the same order of magnitude.

Many experiments have shown that streaks of low-speed/high-speed fluid form near the wall, and that these streaks break down periodically, in which fluid is ejected from the viscous sublayer with significant normal velocities [11], see Fig. 1b. Therefore, in an order of magnitude sense, the time-averaged quantities, $\tau_o(x)$ and $m_o(x)$, are both related to the local density of contact spots defined as:

$$\eta(x)=\frac{\text{cumulative length of direct contact spots}}{\text{total length of sample-wall section}}. \tag{14}$$

The relationship between $\tau_o(x)$ and $m_o(x)$ is:

$$\frac{\tau_o}{\tau_{o,\max}}\sim\eta\sim\frac{m_o}{m_{o,\max}}. \tag{15}$$

Focusing, for the time being, only on extreme ends this relationship and writing the time-averaged τ_o and m in terms of the local coefficients $C_{f,x}$ and h_m/U_∞, it can found that since the direct contact spots are covered wi laminar shear flow and outside these laminar layers t flow and concentration conditions are described by U and C_∞, $\tau_{o,\max}$ and

$$\frac{\dfrac{h_m}{U_\infty}}{\dfrac{1}{2}C_{f,x}}\sim\frac{m_{o,\max}}{C_s-C_\infty}\frac{U_\infty}{\tau_{o,\max}} \tag{16}$$

$m_{o,\max}$ can be obtained from the laminar boundary lay equations:

$$u\frac{\partial u}{\partial x}+v\frac{\partial u}{\partial y}=-\frac{1}{P}\frac{\partial P}{\partial x}+\frac{\mu}{\rho}\left(\frac{\partial^2 u}{\partial y^2}\right) \tag{17}$$

$$u\frac{\partial c}{\partial x}+v\frac{\partial c}{\partial y}=D\left(\frac{\partial^2 c}{\partial y^2}\right). \tag{18}$$

By using the scale analysis method, the scale of $\tau_{o,\max}$ and $m_{o,\max}$ are:

$$\tau_{o,\max}\sim\rho U_\infty^2\left(\frac{U_\infty L}{\nu}\right)^{-1/2} \tag{19}$$

$$\frac{m_{o,\max}}{C_s-C_\infty}\sim\frac{D}{L}Sc^{1/3}\left(\frac{U_\infty L}{\nu}\right)^{1/2}\quad (Sc>1) \tag{20}$$

$$\frac{m_{o,\max}}{C_s-C_\infty}\sim\frac{D}{L}Sc^{1/2}\left(\frac{U_\infty L}{\nu}\right)^{1/2}\quad (Sc<1) \tag{21}$$

where L is the longitudinal length of the boundary shear layer. Combining eqns (16), (20) and (21) and defining $St_m=h_m/U_\infty$, the following scaling law can be obtained:

$$St_m\sim\tfrac{1}{2}C_{f,x}Sc^{-2/3}\quad (Sc>1) \tag{22}$$

$$St_m\sim\tfrac{1}{2}C_{f,x}Sc^{-1/2}\quad (Sc<1) \tag{23}$$

where $C_{f,x}$ is the local skin-friction coefficient, h_m is the mass transfer coefficient, Sc is the Schmidt number ν/D and U_∞ is the free stream velocity. The mass transfer coefficient can be calculated as:

$$h_m\sim\frac{\tau_o}{\rho U_\infty}\left(\frac{\nu}{D}\right)^{-2/3}\quad (Sc>1) \tag{24}$$

$$h_m\sim\frac{\tau_o}{\rho U_\infty}\left(\frac{\nu}{D}\right)^{-1/2}\quad (Sc<1). \tag{25}$$

From the above analysis, it can be seen that the exterior mass transfer coefficient is determined by the boundary

layer flow condition, U_z, wall shear stress, τ_o, and fluid physical properties. The mass transfer rates can be calculated as:

$$m = h_m(C_s - C_z) \tag{26}$$

$$m = \frac{b\tau_o}{\rho U_z}\left(\frac{v}{D}\right)^{-2/3}\left[C_{so}\left(\frac{M(t)}{M_o}\right) - C_z\right] \quad (Sc > 1) \tag{27}$$

$$m = \frac{b\tau_o}{\rho U_z}\left(\frac{v}{D}\right)^{-1/2}\left[C_{so}\left(\frac{M(t)}{M_o}\right) - C_z\right] \quad (Sc < 1) \tag{28}$$

where b is a constant and it is a function of Sc. When $Sc \approx 1$, $b = 1$; otherwise, b has to be obtained from experiments.

In a room or a chamber, the mass balance equation for a VOC or TVOC in the stream air is:

$$V(dC_z/dt) = -QC_z + mA \tag{29}$$

where V is the chamber volume (m^3), Q is the chamber air flow rate (m^3h^{-1}) and A is the source area (m^2). At $t = 0$, $C_z = 0$ (an empty chamber or room) and $M(t) = M_o$. The solution of eqns (27), (28) and (29) give the following expressions for chamber concentration and emission rate:

$$C_z = \frac{b\tau_o}{\rho U_z}\left(\frac{v}{D}\right)^{-2/3}\frac{LC_{so}}{(r_1 - r_2)}(e^{r_1 t} - e^{r_2 t}) \quad (Sc > 1) \tag{30}$$

$$C_z = \frac{b\tau_o}{\rho U_z}\left(\frac{v}{D}\right)^{-1/2}\frac{LC_{so}}{(r_1 - r_2)}(e^{r_1 t} - e^{r_2 t}) \quad (Sc < 1) \tag{31}$$

$$m = \frac{b\tau_o}{\rho U_z}\left(\frac{v}{D}\right)^{-2/3}\frac{C_{so}}{(r_1 - r_2)}[(r_1 + N)e^{r_1 t} - (r_2 + N)e^{r_2 t}] \quad (Sc > 1) \tag{32}$$

$$m = \frac{b\tau_o}{\rho U_z}\left(\frac{v}{D}\right)^{-1/2}\frac{C_{so}}{(r_1 - r_2)}[(r_1 + N)e^{r_1 t} - (r_2 + N)e^{r_2 t}] \quad (Sc < 1) \tag{33}$$

$$r_{1,2} = \left\{-(N + LH + HC_{so}/M_o) \pm [(N + LH + HC_{so}/M_o)^2 - 4NHC_{so}/M_o]^{1/2}\right\}/2 \tag{34}$$

where L is the product loading factor $= A/V$ (m^2m^{-3}), N is the air exchange rate (h^{-1}) and $H = b\tau\rho^{-1}U_z^{-1}(v/D)^{-2/3}$.

In this model, it can be seen that the mass emission rate is determined by fluid properties D, v, and ρ; and fluid conditions U_z, N, L and τ_o. With the exception of the wall shear stress, τ_o, all other parameters can be measured or obtained. Therefore, in this model, there are no coefficients required from data-fitting experimental data from the dynamic chamber or test house studies. Depending on the flow conditions and the geometry, τ_o can be calculated in the following ways:

Wall shear stress calculation (τ_o): The wall shear stress is defined as:

$$\tau_o = \mu\frac{\partial u}{\partial y}\Big|_{y=0} \tag{35}$$

The shear stress of turbulent flow is the summation of both laminar shear stress and turbulence shear stress and they are equal everywhere in a steady state flow,

$$\tau = \tau_w = \mu\frac{\partial u}{\partial y} + \rho u'v'. \tag{36}$$

This shows that the wall shear stress of turbulent flow depends not only on the mean flow velocity, but also on the turbulent flow condition. Depending on the flow condition and geometry, there are different relationships existing between the wall shear stress and flow condition. As mentioned before, both velocity and concentration boundary layers on a non-slip solid surface have been visualized as two sublayers: (1) the laminar sublayer, where $v > \varepsilon$, and (2) the inertial sublayer (fully turbulent sublayer) where $\varepsilon \gg v$. In the inertial sublayer, eqn (36) can be rewritten as:

$$\tau = \tau_o \cong \rho u'v'. \tag{37}$$

From experiments, the following empirical relationship has been obtained in the inertial sublayer [12]

$$\tau_o \cong \rho\overline{u'v'} \cong 0.4u'v'. \tag{38}$$

As turbulence is stochastic in nature, it is only possible to calculate the wall shear stress theoretically for some ideal cases, such as flow over smooth pipes and semi-infinite flat plates [13]. Von Karmen devised an expression for the calculation of skin friction for the case of uniform fluid flowing over a smooth semi-infinite flat plat [13]:

$$C_{f,x} = 0.664Re_x^{-1/2} \quad (\text{Laminar flow, } Re_x < 10^5, \text{Local}) \tag{39}$$

$$C_{f,L} = 1.328Re_L^{-1/2} \quad (\text{Laminar flow, } Re_x < 10^5, \text{Average}) \tag{40}$$

$$C_{f,x} = 0.0592Re_x^{-1/5} \quad (\text{Turbulent flow, } 5*10^5 < Re_x < 10^8, \text{Local}) \tag{41}$$

$$C_{f,L} = 0.074Re_L^{-1/5} - 1742Re_L^{-1} \quad (\text{Turbulent flow, } 5*10^5 < Re_x < 10^8, \text{Average}) \tag{42}$$

$$C_f = \frac{\tau_o}{1/2\rho U_z^2} \tag{43}$$

where $Re_L = U_\infty L/\nu$ and L is the characteristic length of the flat plate.

Most material surfaces cannot be regarded as smooth surfaces, so that the velocity distribution, resistance to the flow, boundary layer thickness and wall shear stress are effected by the roughness of surfaces. Schlichting [13] stated that rough surfaces can be classified into three groups based on their effect on the flow.

2.2.1. Hydraulically smooth

In this category, the height of protrusions caused by the roughness is smaller than the thickness of the laminar sublayer, thus, the roughness has little effect on the flow. Examples of these are polished wood and commercial steel.

$$0 < \frac{k_s u_\tau}{\nu} < 5 \quad \tau_o = \tau_{o,\text{smooth}} \tag{44}$$

where k_s is the sand roughness and U_τ is the friction velocity, $(\tau_o/\rho)^{1/2}$.

2.2.2. Transition

Protrusions extended partly outside the laminar sublayer, and additional resistances, as compared with smooth pipe, are mainly due to the formed drag experienced by the protrusion in the boundary layer.

$$5 \leqslant \frac{k_s u_\tau}{\nu} \leqslant 70 \quad \tau_o = f \quad \text{(roughness, flow condition)}. \tag{45}$$

2.2.3. Completely rough

All protrusions reach outside the laminar sub-layer and by far the largest part of the resistance to flow is due to the formed drag which acts on them.

$$70 \leqslant \frac{k_s u_\tau}{\nu} \quad \tau_o = f \quad \text{(roughness)}. \tag{46}$$

By using the appropriate equation or empirical expression mentioned above, surface shear stress τ_o in most flow conditions over a surface can be calculated. Thus, the emission rate can then be calculated by using eqns (27) and (28).

3. Model validation

The validation of this model was performed by comparing its predictions against the experimental results from the Centre for Building studies (CBS). Concordia University, experimental results from the U.S Environmental Protection Agency (EPA), as well as the predictions made by other models.

3.1. Model validation with the experimental results from the velocity controlled test chamber

The model was first tested against the experimental results from both a constant source, water, and a fast-decay wet source, varnish. These results were obtained in a CBS velocity controlled test chamber [14].

The small velocity-controlled test chamber is made of stainless steel and consists of two parts: a rectangular chamber area and a cone shaped part as shown in Fig. 2. The test area is located in the rectangular chamber, and an uniform airflow is generated here. The purpose of the cone shape is to help strengthen the flow in the chamber area and to thoroughly mix the exit air. At the junction of these two parts, there are two fans (Sunon Brushless Blower OD 5.5 cm) installed at a distance of 100 mm from either side of the wall. A stainless steel mesh screen with mesh size 7.5 cm^{-1} is placed directly before the fans.

These fans are installed to draw air through the test chamber; while the stainless steel mesh helps to provide uniform flow in the test area. A TFE-fluorocarbon tube mesh or a stainless steel mesh is positioned at the inlet of the test chamber to generate a homogeneous and isotropic turbulence with different levels of turbulent fluctuations. A height adjustable test area is designed to prevent emissions from the edge of the testing materials and to avoid disturbances to the flow pattern caused by the thickness of the testing materials. The test area measures 250 by 200 mm, and is located 100 mm downstream from the inlet, at the centre of the cross section. The test chamber is constructed such that its bottom includes a 250 by 200 mm indented area (see Fig 2(a)). Within the indented area, there is a stainless steel plate, the size of the test area, which can be raised or lowered from 0 to 10 mm below the chamber bottom by tightening or loosening screws. While this adjustment accommodates for the thickness of the materials, the indented area ensures no leakage.

This small velocity-controlled test chamber can be operated at three different levels of turbulent fluctuations. To achieve the first level, a TFE-fluorocarbon tube mesh, which is made of a set of teflon tubes with diameter of 10 mm and depth of 5 cm arranged in a honeycomb configuration, is installed at the inlet of the test chamber. For the second level, a coarse stainless steel mesh with grid 7.5 cm^{-1} replaces the TFE-fluorocarbon tube mesh at the inlet. The third level uses a fine stainless steel mesh with grid 11.4 cm^{-1}. For each level of turbulent fluctuation, there exists a relationship between the fan power reading and the mean air velocity inside the test chamber. At all levels of turbulent fluctuations, both the mean flow condition and the boundary layer over the test area are designed to be uniform.

A series of air velocity measurements were performed in order to characterize the velocity-controlled test chamber and to verify that the objectives of the design were

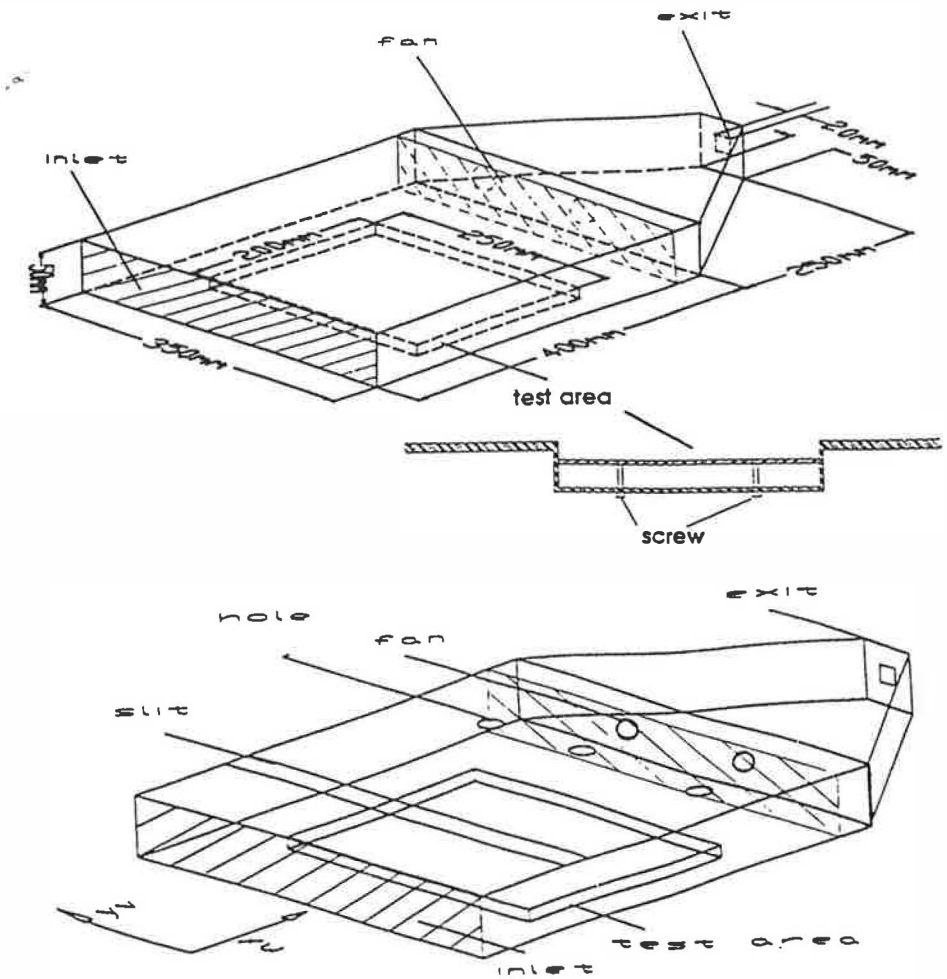

Fig. 2. (a) The small air velocity controlled test chamber designed at the CBS. (b) The model of the small velocity-controlled test chamber for calibration.

achieved. A Dantec 60× dual beam Laser Doppler Velocimetry (LDV) (TSI Model No. 9100-3) was used to measure the velocity. LDV has a lower measuring limit of 0.001 ms^{-1} and it uses water vapour as particles for detection; water vapour is generated by the SUPER Ultrasonic SH550T.

For better visualization and convenience in taking velocity measurements, a polymethylmethylacrylate (PMMA) chamber model, identical to the small velocity-controlled test chamber, was built for the characterization. To avoid the distortion of the laser light, calibrating measurements were taken at the top plate of the model where a 25 mm slit was cut at a location of 150 mm from the inlet. Also, three 10 mm diameter holes were drilled at the rear edge of the test area, as shown in Fig. 2(b). Except for the measuring points, the slit and holes were normally blocked with removable covers. The measurements were carried out under steady-state conditions. The steady state condition is indicated by steady air velocity and turbulent fluctuation readings (the difference between readings is within a 5% discrepancy) [15].

3.1.1. Constant source

The model—eqns (27) and (28)—was first validated using the experimental results from the velocity controlled test chamber with a constant emission source, water. For constant sources, $C_{so} = C_o$. The air flow in the velocity controlled test chamber is a parallel flow and both the velocity and the turbulence level are very low. Therefore, the air flow is treated as laminar flow over a flat plate, and the wall shear stress, τ_o, is calculated using eqns (40) and (43). The physical properties of water used in the model validation are listed in Table 1 [16].

Table 2 shows the comparison of the model predictions with the experimental results. It can be seen that the predicted values are in good agreement with the experimental results, with the maximum error between the two within ±20%.

3.1.2. Wet source

The model was then validated by using the varnish test results from the small velocity controlled test chamber [15]. The air flow inside the chamber is treated as laminar

Table 1
Physical properties of water and chamber parameters

Physical properties	
Air density ρ	1.185 kgm^{-3}
Air viscosity ν	15.89×10^{-6} m^{2}s^{-1}
Diffusivity$_{\text{water vapour-air}}$ D	2.56×10^{-5} m^2 s^{-1}
Saturated vapour concentration C_w	0.0224 kgm^{-3}
Sample surface area	0.039 m^2
Chamber dimension	$0.04 \times 0.035 \times 0.005$ m^3

flow over a flat plate. The physical properties of the varnish [17] are listed in Table 3.

Figures 3–6 show the comparison of the predicted varnish emission rates with the experimental results at different surface air flow conditions. There are some discrepancies between predicted emission rates and experimental ones during the initial hours (due to initial experimental instability), and the predicted results tend to be higher than the experimental ones at the end of the test (due to the gas chromatograph's limitation in detecting low levels of VOC). In spite of this, the predicted results and experimental results closely follow the same trend, especially for the low velocity cases. For the higher velocity cases, greater discrepancies between model predicted results and experimental results are noticed. This was caused by the effects of the turbulent fluctuation, which became more significant as the velocity increased, even though theoretically the flow is still in the laminar range. The effects of the turbulent fluctuation were not fully reflected in the model since laminar flow over a flat plate was assumed.

3.2. Further validation of the proposed model with experimental data in literature

The model predictions were also compared with experimental data obtained at the EPA using an ASTM standard small test chamber. A fan was installed to mix the air inside the chamber and to create the different levels of surface air velocity and turbulent fluctuation. It is a mimic model of a real room situation. In such a case, the near wall flow in a room or a room-like chamber is a two dimensional flow parallel to the surface [18]. As the maximum Reynolds number is around 9000 ($\ll 5 \times 10^4$, the critical Reynolds number for flow over a flat plate) in the tests, in the following model predictions, the wall shear stress, τ_o, is treated as laminar flow over a flat plate, as was done in the previous cases.

3.2.1. Constant source

The model—eqns (32), (33) and (34)—was validated by the EPA experimental results from p-dichlorobenzene crystals, a constant source [17]. The experiments were conducted in the ASTM standard chamber at different surface air velocity levels, but at a constant air exchange rate of 0.5. The physical properties of p-dichlorobenzene, chamber parameters and flow conditions used in the model prediction are listed in Table 4. The experimental conditions and results, as well as predicted results, are shown in Table 5. It can be seen that the predicted results and the experimental results are in good agreement, with the maximum error less than 20%.

3.2.2. Wet source

The physical model was further validated using the test results from polyurethane in the ASTM standard test chamber [7]. Two sets of experimental concentration versus time data, obtained for two different initially applied

Table 3
Physical properties for varnish tests

Physical properties	
Air density ρ	1.185 kgm^{-3}
Air viscosity ν	15.89×10^{-6} m^{2}s^{-1}
Diffusivity$_{\text{TVOC-air}}$ D	2.56×10^{-5} m^2 s^{-1}
Saturated vapour concentration C_w	0.0224 kgm^{-3}

Table 2
Comparison of the predicted results with water emission test results

Vel. (ms^{-1})	R.M.S. (ms^{-1})	Temp. (C)	C_{in} (gm^{-3})	C^*_{out} (gm^{-3})	M_{exp} (gm^{-2}s^{-1})	M_{cal} (gm^{-2}s^{-1})	Error (%)
0.053	0.0094	24.2	5.76	6.88	0.00106	0.00089	16
0.058	0.0066	24.3	5.84	6.96	0.00117	0.00093	21
0.053	0.0025	24.2	5.96	7.08	0.00106	0.00088	17
0.095	0.0088	24.5	5.88	6.69	0.00138	0.00119	13
0.087	0.0070	24.6	5.93	6.69	0.00120	0.00114	4
0.091	0.0028	24.7	6.14	6.96	0.00134	0.00115	14
0.114	0.0114	24.6	6.03	6.74	0.00147	0.00130	11
0.114	0.0072	24.6	5.91	6.51	0.00125	0.00132	5
0.113	0.0034	24.4	6.06	6.71	0.00134	0.00130	3

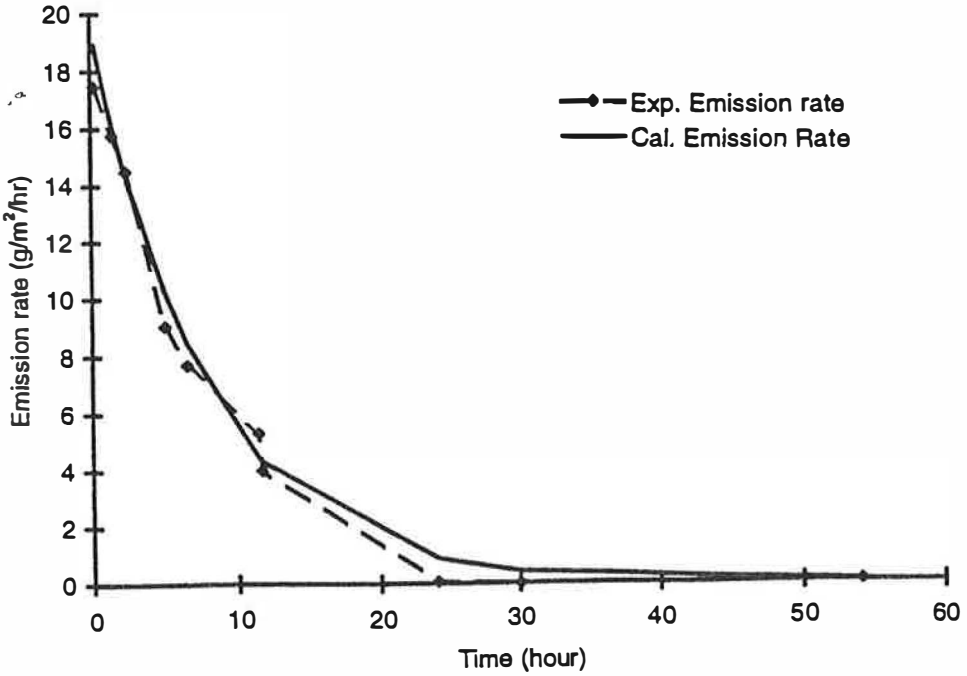

Fig. 3. Predicted and experimental data of the VOC concentration vs time for varnish at velocity = 0.053 ms^{-1} and R.M.S. = 0.0025 ms^{-1}.

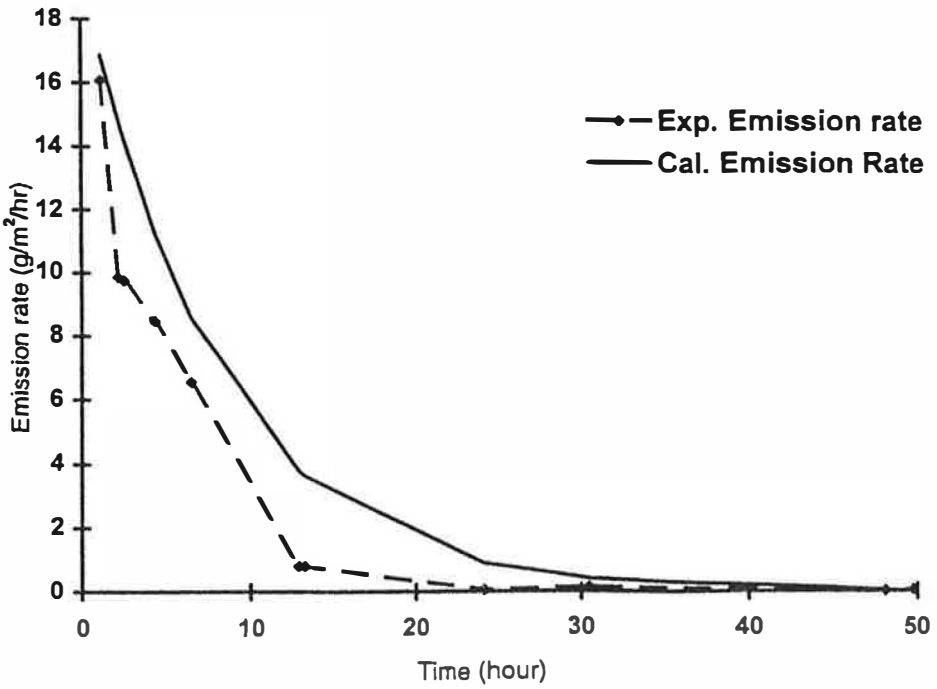

Fig. 4. Predicted and experimental data of the VOC concentration vs time for varnish at velocity = 0.053 ms^{-1} and R.M.S. = 0.0094 ms^{-1}.

amounts of polyurethane, were supplied by the EPA. The physical properties, chamber parameters and flow conditions used in the calculation are listed in Table 6.

Figures 7 and 8 compare the model predicted chamber TVOC concentrations with the experimental ones. It can be seen that at the beginning of the curves, the model predicts higher TVOC concentrations than the measured values; and at the tail-end, the model underestimates the TVOC concentrations in the chamber. This phenomena may be explained by two factors. The

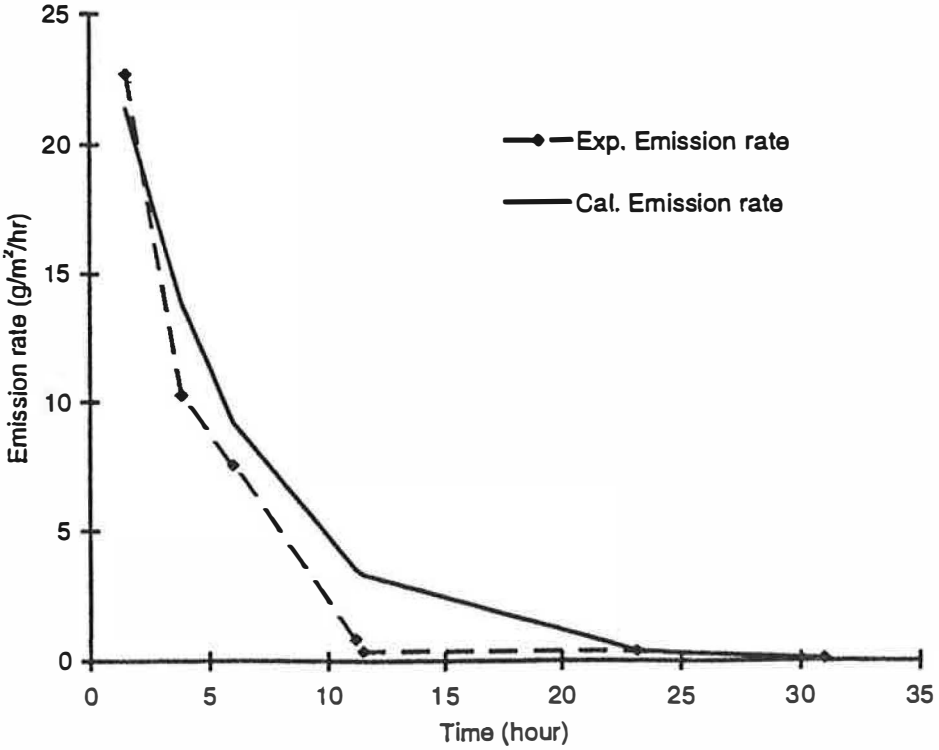

Fig. 5. Predicted and experimental data of the VOC concentration vs time for varnish at velocity = 0.113 ms^{-1} and R.M.S. = 0.0034 ms^{-1}.

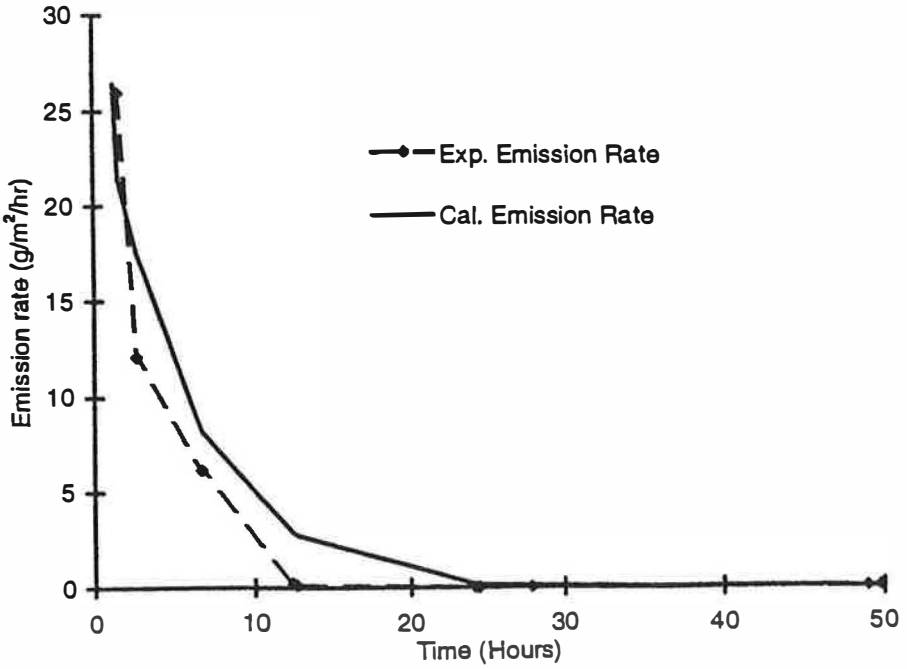

Fig. 6. Predicted and experimental data of the VOC concentration vs time for varnish at velocity = 0.113 ms^{-1} and R.M.S. = 0.0114 ms^{-1}.

first factor is the sink effects occurring in both the wood substrate and the steel chamber. In particular, the wood substrate, acting as a sponge, absorbs the polyurethane into its interior at the beginning of the test and releases it later. The other factor is the instability and partial mixing in the chamber at the beginning of the tests. However, over all, the predicted curves follow the experimental ones closely.

Table 4
Physical properties and chamber parameters for the p-dichlorobenzene tests

Product name—p-dichlorobenzene crystal	
Physical properties	
Air density ρ	1.185 kgm^{-3}
Air viscosity ν	15.89×10^{-6} m^{2}s^{-1}
Diffusivity$_{TVOC-air}$ D	5.75×10^{-6} m^{2}s^{-1}
Initial Concentration C_{so}	0.0217 kgm^{-3}
Chamber parameters and flow conditions	
Air exchange rate	0.5268 h^{-1}
Surface air velocity	0.03 ms^{-1}
Sample surface area	0.021 m^2
Chamber volume	0.053 m^3
Substrate	A plastic cylindrical container

Table 6
Physical properties, chamber parameters and flow conditions for the polyurethane tests

Product name—Naso polyurethane wood finish	
Physical properties	
Air density ρ	1.185 kgm^{-3}
Air viscosity ν	15.89×10^{-6} m^{2}s^{-1}
Diffusivity$_{TVOC-air}$ D	5.75×10^{-6} m^{2}s^{-1}
Initial concentration C_{so}	0.0217 kgm^{-3}
Chamber parameters and flow conditions	
Air exchange rate	0.5268 h^{-1}
Surface air velocity	0.03 ms^{-1}
Sample surface area	0.021 m^2
Chamber volume	0.053 m^3
Initial mass	0.96 and 1.82 g
Net loss	0.58 and 0.76 g
Substrate	Smooth oak board

3.3. Inter-model comparison

The emission rates predicted by the proposed physical model were also compared with results predicted by other existing models: first-order decay model [19] and the EPA's mass transfer model [7]. As shown in Fig. 9, the predictions of the emission rate from polyurethane made by the proposed model fit the experimental data better than the predictions made by the empirical first-order decay model. As mentioned earlier, the coefficients of the empirical first-order model were obtained from experiments, and are only valid for the material and conditions under which the experiment was performed.

Figure 9 also shows the predictions made by the EPA's mass transfer model. It appears that the EPA's model fits the experimental data slightly better than the proposed physical model. The reason for this is that the EPA model requires the boundary layer thickness, δ, as its input. This coefficient is obtained through data-fitting the same experimental data. Therefore, this value may be the apparent boundary layer thickness rather than the real boundary layer thickness. On the contrary, the proposed model does not require any input from experimental results; it is completely independent of experimental data.

4. Conclusion

A mathematical model, based on the fundamental fluid flow and mass transfer theories, has been developed to predict VOC emission rates from homogeneous materials. One of the unique features of the proposed model is that it considers both mass diffusion and mass convection in the boundary layer between the material surface and the air flow. This makes the relationship between the surface air flow and material emission rates obvious and enables the model to predict material emission rates under different environmental conditions. The other feature of the proposed physical model is that all the parameters have clear physical meaning and can be either found in literature, calculated using known theories and/or equations.

At present, the existing models, both empirical and physical, require data from dynamic chamber experiments in order to obtain certain coefficients, and are limited to the experimental conditions under which the coefficients were obtained. Five to ten samples are needed to ensure a valid curve fit for such experiments. Therefore,

Table 5
Comparison of experimental and predicted results from p-dichlorobenzene crystals

	Vel. (ms^{-1})	Temp. (°C)	C (gm^{-3})	C_{sat} (gm^{-3})	M_{test} (gm^{-2}s^{-1})	M_{cal} (gm^{-2}s^{-1})	Error (%)
1	0.03	23.0	2.03	12.74	0.0035	0.0042	17
2	0.09	23.2	3.67	12.74	0.0061	0.0062	1
3	0.14	23.4	4.60	12.74	0.0077	0.0069	11
4	0.23	23.0	5.06	12.74	0.0087	0.0084	4
5	0.46	23.0	5.51	12.74	0.0093	0.011	16

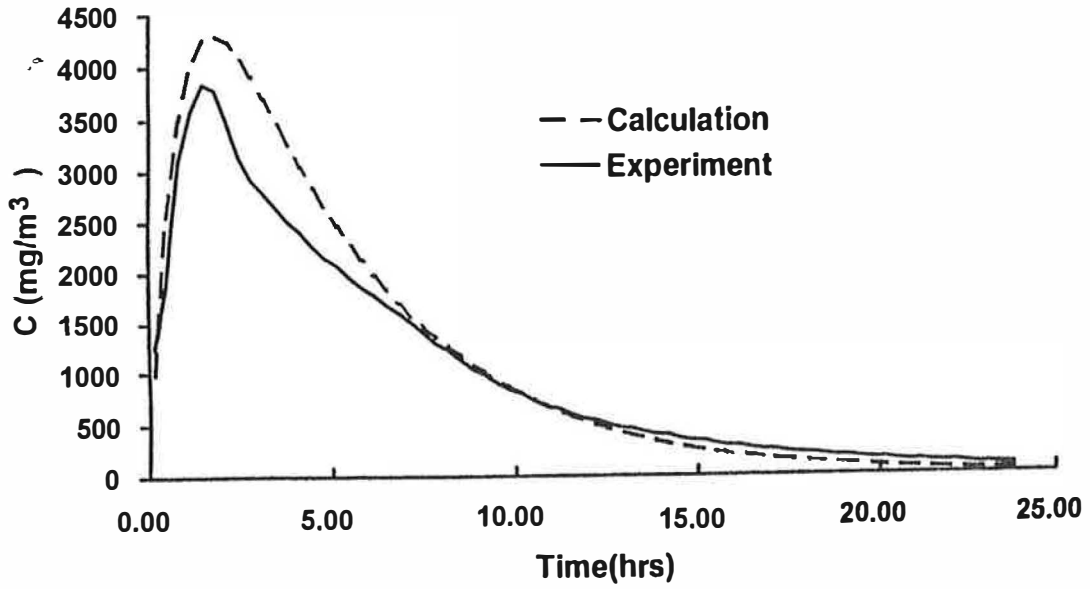

Fig. 7. Predicted and experimental data for the VOC concentration vs time for polyurethane at initial applied amount of 0.96 g.

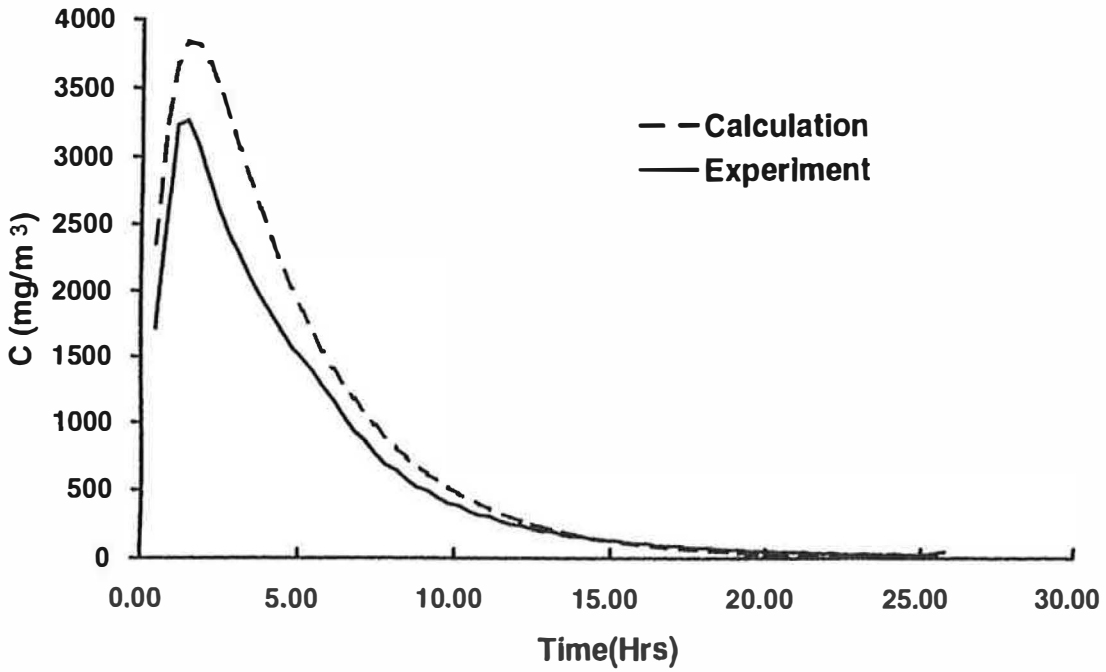

Fig. 8. Predicted and experimental data for the VOC concentration vs time for polyurethane at initial applied amount of 1.82 g.

with the development of this proposed model, the emission rate can be obtained without expensive and difficult dynamic chamber testing, and may result in a simpler and less expensive way to determine the material emission strength.

The predictions made by this model were validated at three different levels; with experimental results from the CBS specially designed test chamber, with experimental results from the EPA which were carried out in an ASTM chamber, and finally with the predictions made by other models. The results indicate that there is, in general, good agreement between the model predictions and the experimental results. The main advantage of this model is that the model does not require any experimental data as input.

Since the model is based on several assumptions, no chemical reactions, no temperature difference, no sink effects, etc. Such assumptions may cause errors when the model is applied to the real indoor environment. Further research on these aspects is needed.

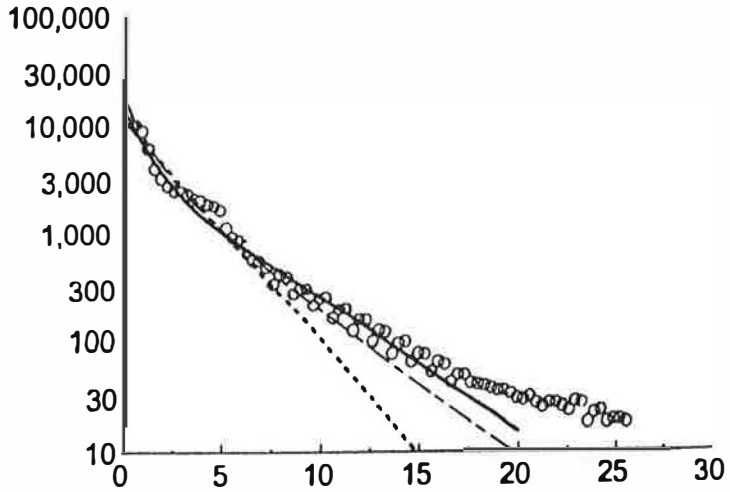

Fig. 9. Polyurethane (applied amount of 1.82 g) emission rates predicted by the EPA mass transfer, first-order decay and the proposed physical models.

Acknowledgements

This study was supported by a grant from the Natural Sciences and Engineering Research Council, Canada. We wish to thank Dr B. A. Tichenor of the U.S. Environmental Protection Agency (EPA) for providing the experimental data.

References

[1] Tichenor BA, Guo Z, Spark LE. Fundamental mass transfer model for indoor air emissions from surface coating. Indoor Air 1993;3:263–8.
[2] Colombo A, Bortoli DM. Comparison of models used to estimate parameters of organic emissions from materials tested in small environmental chambers. Indoor Air 1992;2(1):49–57.
[3] Andersen I, Lundquist GR, Molhave L. Indoor air pollution due to chipboard used as a construction material. Atmospheric Environment 1975;9:1121–7.
[4] Hoetjer JJ. Introduction to a theoretical model for the splitting of formaldehyde from composition board. Report Method Chemie Netherlands, Delfzijil 1978.
[5] Black MS, Bayer CW. Formaldehyde and other VOC exposures from consumer products. Proceedings of IAQ 1986, Atlanta, GA: American Society of Heating Refrigerating, and Air-conditioning Engineers, Inc. 1986. p. 454–486.
[6] Dunn JE, Tichenor BA. Compensation for sink effects in emission test chambers by mathematical modelling. Atmospheric Environment 1988;22(5):885–94.
[7] Guo ZS, Tichenor BA. Fundamental mass transfer models applied to evaluating the emissions of vapour-phase organic from interior architectural coatings. Preceedings of EPA AWMA Symposium, Durham, NC, 1992.
[8] Haghighat F, De Bellis L. Material emission rates: literature review, and the impact of indoor air temperature and relative humidity. Building and Environment 1998;33(5):261–277.
[9] Sparks LE, Tichenor BA, Chang J, Guo Z. Gas-phase mass transfer model for predicting volatile organic compounds (voc) emission rates from indoor pollutant sources. Indoor Air 1996;6:31–40.
[10] Narazoff WW, Cass GR. Mass-transport aspects of pollutant removal at indoor surfaces. Environment International 1989;15:567–84.
[11] Bejan A. Convection heat transfer. John Wiley and Sons, 1984.
[12] Tennekes H, Lumley JL. A first course in turbulence. Cambridge, Massachusetts, England, 1970.
[13] Schlichting H. Boundary-layer theory. 7th edn. McGraw-Hill, 1979.
[14] Zhang Y, Haghighat F. A small air velocity-controlled test chamber for emission studies. Proceedings of Symposium of Methods for Characterizing Indoor Sources and Sinks, Washington, D.C., 25–28 September 1994.
[15] Zhang Y, Haghighat F. The impact of surface air movement on material emissions. Building and Environment 1997;32(6):551–6.
[16] ASHARE Handbook. Fundamentals. Atlanta, GA: American Society of Heating, Refrigeration and Air Conditioning Engineers, 1993.
[17] Guo Z, Tichenor BA, Krebs KA, Roache NF. Consideration on revisions of emissions testing protocols. Proceedings of the Symposium of Methods for Characterizing Indoor Sources and Sinks, Washington, D.C., 25–28 September 1994.
[18] Haghighat F, Jiang Z, Zhang Y. The impact of ventilation rate and partition layout on VOCs emission rate: Time-dependent contaminant removal. Indoor Air 1994;4:276–83.
[19] Tichenor BA. Indoor air sources: Using small environmental test chambers to characterize organic emissions from indoor materials and products. EPA-600/8-89-074, U.S. Environmental Protection Agency, Research Triangle Park, NC, August, 1989.